Quaternary Geochronology 49 (2019) 115–122

Contents lists available at ScienceDirect

Quaternary Geochronology

journal homepage: www.elsevier.com/locate/quageo

Research paper

Single-grain OSL dating of fluvial terraces in the upper Hunter catchment, southeastern Australia

Xiao Fu[a,*], Tim J. Cohen[b,c], Kirstie Fryirs[d]

[a] Centre for Archaeological Science, School of Earth and Environmental Sciences, University of Wollongong, Wollongong, NSW, 2522, Australia
[b] GeoQuEST Research Centre, School of Earth and Environmental Sciences, University of Wollongong, Wollongong, NSW 2522, Australia
[c] ARC Centre of Excellence for Australian Biodiversity and Heritage, University of Wollongong, Wollongong, NSW 2522, Australia
[d] Department of Environmental Sciences, Macquarie University, North Ryde, NSW 2109, Australia

ARTICLE INFO

Keywords:
Fluvial terrace
Southeastern Australia
Single-grain OSL
Single-grain rejection criteria
Glacial episode
LGM

ABSTRACT

Fluvial terraces in the upper Hunter catchment, southeastern Australia provide a long-term record of river activity in response to climate change in the late Quaternary. Single-grain optically stimulated luminescence (OSL) dating of quartz was applied in this study to investigate the timing of the formation of three fluvial terraces in the upper Hunter catchment. A detailed examination of luminescence properties of individual quartz grains revealed some correlation between their OSL decay rates, intrinsic brightness and dose saturation characteristics. Some quartz grains containing a higher proportion of non-fast components exhibit low brightness in OSL signals and high dose saturation levels. Some grains with slow OSL decays pass the standard rejection criteria, but are likely to yield underestimated equivalent doses (D_es) because of a higher contribution of non-fast components, which are shown to have low thermal stability. Different rejection criteria, including the fast ratio, the dose saturation level and the OSL sensitivity criteria, were tested on the single-grain D_e results. Application of a fast ratio rejection criterion is able to successfully identify thermally unstable grains. A new rejection criterion based on dose saturation property was also applied to improve the age of one sample with a large D_e. Our dating results identify multiple phases of river valley aggradation in the upper Hunter catchment since late Marine Isotope Stage (MIS) 6; at ~ 138 ka, ~90–94 ka, ~65 ka, ~26 ka and ~18 ka. The aggradational episodes of the terraces in the upper Hunter catchment are correlated with glacial or stadial periods since MIS 6. These phases of valley-floor aggradation are inferred to be a function of increased sediment supply during the cold periods resulting from strong periglacial activities in the adjacent Australian highlands.

1. Introduction

Fluvial sediments in Australia have provided important archives for assessing late Quaternary flow regime changes (e.g. Nanson et al., 1992). In southeastern Australia, abundant evidence exists of enhanced runoff conditions (relative to today) throughout the last full glacial cycle. A number of previous studies in this region have focused on large inland rivers draining west from the Great Dividing Range (GDR) which provides a record of river activity since Marine Isotope Stage (MIS) 5 (e.g. Nanson et al., 1992; Page et al., 1996, 2009; Kemp and Rhodes, 2010; Kemp et al., 2017). However, for the coastal draining catchments to the east of the GDR, the available fluvial record is less constrained and mostly shorter given the narrow valleys and resulting poorer preservation potential. In eastern New South Wales (NSW), the hydrological setting is characterized by a series of smaller coastal-draining catchments ($< 1000\,km^2$) surrounded by much larger basins, such as the Hunter and Shoalhaven catchments which extend to the west of the great escarpment and with drainage areas $> 5000\,km^2$ (Fig. 1a). Previous studies have focused on small coastal valleys which mainly record post-Last Glacial Maximum (LGM) and Holocene valley-floor accumulation (e.g. Fryirs and Brierley, 1998; Brooks et al., 2003; Cohen and Nanson, 2008). Fewer studies (Nott et al., 2002; Nanson et al., 2003) have investigated the much larger catchments containing drainage areas above the escarpment (on the tablelands), despite preserving antecedent fluvial landforms of much greater antiquity (e.g. Nott et al., 2002). The reliable determination of ages of such terraces is important for exploring the reconstruction of long-term flow-regime changes east of the GDR and forms the basis for understanding the regional palaeoclimatic variations of southeastern Australia; optically stimulated luminescence (OSL) technique offers an effective tool to date the formation of river terraces (e.g. Zhang et al., 2009; Meng et al., 2015; Fu et al., 2017b).

* Corresponding author.
E-mail addresses: xiaofu@uow.edu.au, xiaofuled@gmail.com (X. Fu).

https://doi.org/10.1016/j.quageo.2018.06.002
Received 30 November 2017; Received in revised form 12 March 2018; Accepted 3 June 2018
Available online 04 June 2018
1871-1014/ © 2018 Elsevier B.V. All rights reserved.

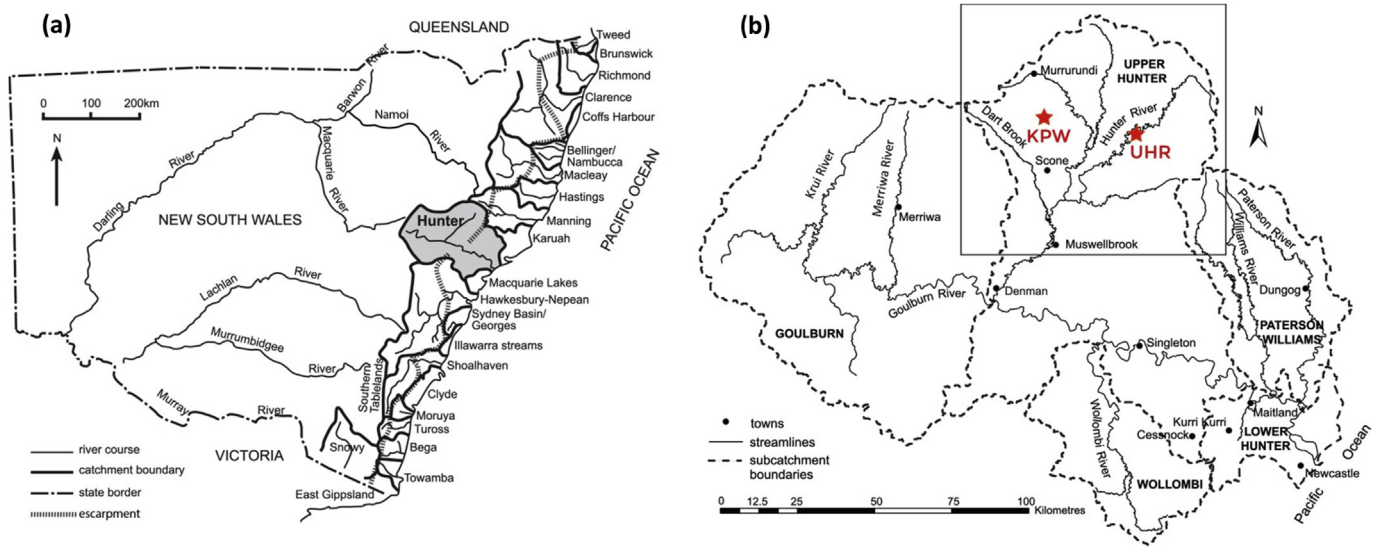

Fig. 1. (a) Map showing the coastal catchments of New South Wales, Australia and the location of the Hunter catchment. (b) Map of the Hunter catchment. The square indicates the location of the upper Hunter catchment. Stars indicate the locations of the sampling sites: UHR—Upper Hunter at Razorback; KPW—Kingdon Ponds at Wingen (Fryirs, unpublished data).

This paper presents a detailed single-grain OSL dating study for three fluvial terraces preserved in the upper Hunter catchment, the third largest coastal draining catchment in NSW. We report the characteristics of the OSL signals of individual quartz grains for the upper Hunter samples, as well as the sensitivity of their equivalent dose (D_e) estimates to different newly proposed single-grain rejection criteria (e.g. Duller, 2012). The new terrace chronologies are compared with climate cycles and existing fluvial records in the study region, and the implications for river responses to palaeoclimate changes are discussed.

2. Study sites and samples

The Hunter catchment is located on the central coast of NSW with an area of 22,000 km^2 (Fig. 1a and b). It is one of the largest catchments in coastal NSW and extends west of the great escarpment in eastern Australia. This larger catchment, and specifically the upper Hunter, is located very near the headwaters of the Macquarie River, a major subcatchment of the Murray-Darling Basin (MDB). Therefore the larger Hunter catchment shares morphological and climatic characteristics of the smaller coastal catchments but is also well situated to headwater rivers of the MDB from which the long record of flow-regime changes exist.

The upper Hunter catchment is located in the northeastern region of the basin (Fig. 1b) and most of the rivers in the catchment are classified as confined or partly-confined. In these settings, lateral movement of the contemporary river courses are confined by bedrock valley margins or antecedent landforms formed under former flow regimes, such as fluvial terraces and alluvial fans (Fryirs and Brierley, 2010). These antecedent landforms not only provide confinement for modern river behaviour, but also record a long history of fluvial activity.

In this study we sampled three fluvial terrace sections in the upper Hunter catchment. Two fluvial terrace exposures, named the Razorback upper terrace and lower terrace, are located near the Razorback Bridge in the central east of the upper Hunter catchment (Fig. 1b). The terraces are ~600 m away from each other and are 10–13 m above the modern river channel (Fig. 2b and d); and are located on the convex margin of the meander bends or at the channel inflection point. The Razorback upper terrace is mainly composed of massive silty clay, overlying a thin unit of channel gravels with no bedrock exposed at the base of exposure (Fig. 2a). One OSL sample UH-URB was collected from the lower part of this section. Three stratigraphic units were identified from the Razorback lower terrace, including a bedrock strath at the base, overlain by a coarse gravel to cobble channel facies, underlying a silty clay channel-fill unit (Fig. 2c). One sample UH-LRB was collected from the silty clay unit immediately above the gravel dominated channel facies.

The third sampled fluvial terrace section is on Kingdon Ponds at Wingen (Fig. 1b), a tributary in the central west of the upper Hunter catchment. This terrace (named the Kingdon Ponds terrace) is 10 m above the current channel bed (~5 m above the floodplain) (Fig. 2f) and is characterised by a complex stratigraphy of gravels and finer-grained facies (Fig. 2e). The basal unit is a gravel lag (Unit A) underlying a cemented silty-clay unit at the bottom of the section (Unit B). Above the silty-clay unit is a complex stratigraphy of gravel-dominated facies comprising channel fill, trough-cross beds, matrix-supported massive and horizontally bedded units. These units reflect various phases of bar development and cut-and fill (Units C1-D3) that are terminated by debris flow deposits (Units E1-E2). Atop the debris flow units is a vertically accreted floodplain surface (Units F1-F3) but with coarse-grained lenses. Five samples KPW-1 to KPW-5 were collected from Units F1 to B from top to the bottom.

3. Methods

Single-grain quartz OSL dating was performed for all samples. OSL samples were prepared using the same method as detailed in Fu et al. (2017a). Sand-sized (180–212 μm or 212–250 μm in diameter) quartz grains were separated and then etched for 40 min using 45% HF acid. OSL was measured on a Risø DA-20 TL/OSL reader. The OSL signals of individual grains were obtained by stimulation using a focused 10 mW green (532 nm) laser at 125 °C for 1.8 s, and collected using an EMI9235QA photomultiplier tube through 7.5 mm Hoya U-340 filter. A single-aliquot regenerative dose (SAR) protocol (Murray and Wintle, 2000) was used to determine the D_es of individual grains, which includes an IR depletion-ratio test (Duller, 2003) applied to each grain at the end of the SAR sequence (using an infrared exposure of 100 s at 50 °C) to detect any potential feldspar contamination. Based on dose recovery tests, the preheat temperatures for samples from the Razorback terraces and Kingdon Ponds terrace were chosen to be 240 °C and 220 °C, respectively.

All luminescence data were processed using the **R** packages 'numOSL' (Peng and Li, 2017) and 'Luminescence' (Kreutzer et al., 2017). The net OSL signal was calculated from the first 0.2 s of the OSL

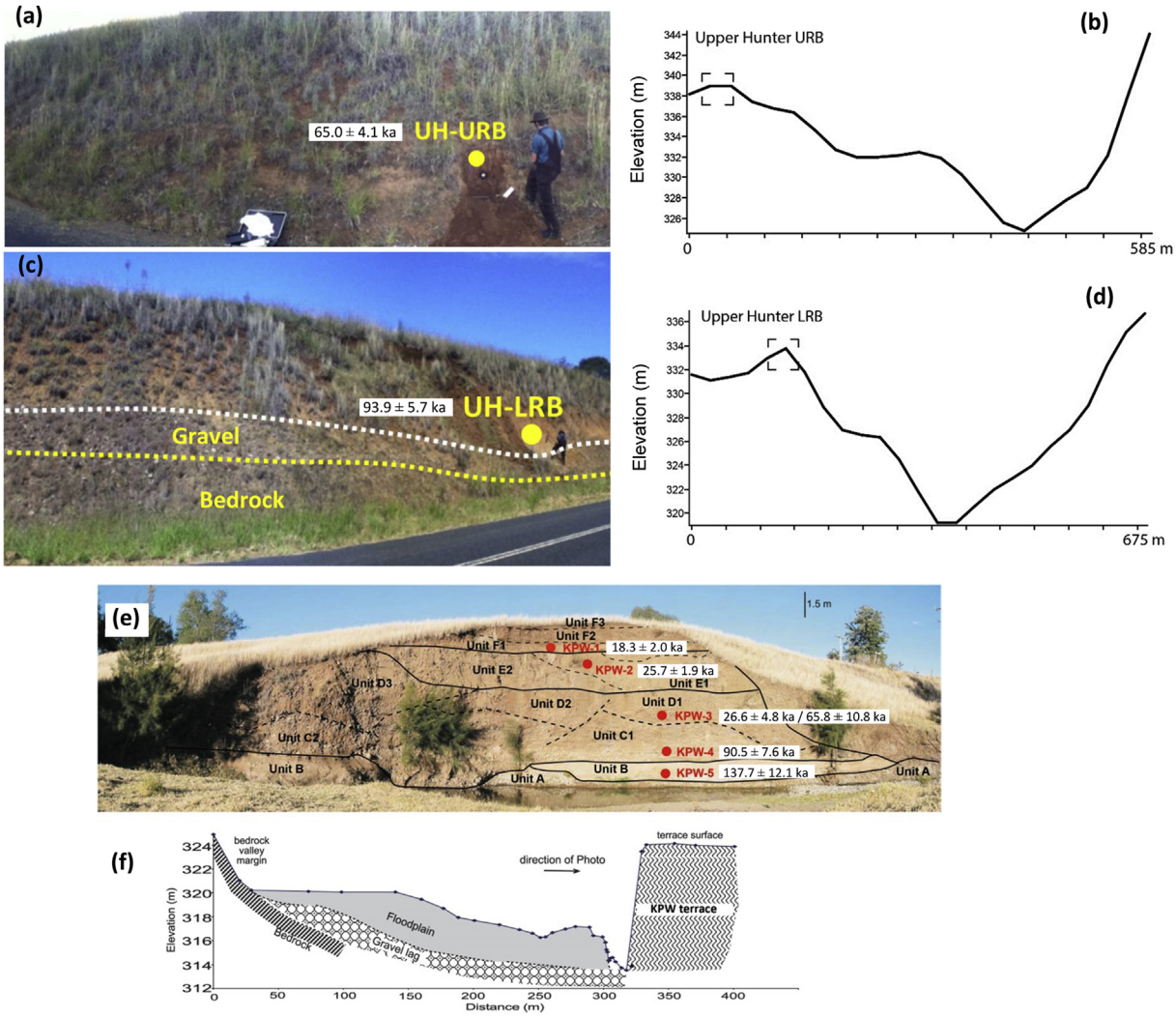

Fig. 2. (a) Photograph showing the Razorback upper terrace exposure. (b) Transect of the Razorback upper terrace generated from the SRTM 30 m digital elevation model (DEM). (c) Photograph showing the Razorback lower terrace exposure. (d) Transect of the Razorback lower terrace generated from the SRTM 30 m DEM. (e) Photograph showing the Kingdon Ponds terrace exposure with unit boundaries (solid black line) and tentative unit or sub-unit boundaries (dashed line). Unit A is the basal gravels, Unit B is a fine-grained cemented facies, Units C1 to E2 are comprised of cobble and gravel units – mostly matrix-supported. Units F1-F3 includes thin gravel and sand lenses underlying fine-grained overbank material. (f) Valley cross-section showing the geomorphic setting of the Kingdon Ponds terrace (Fryirs, unpublished data). Elevations in (b), (d) and (f) are expressed as Australian Height Datum (AHD) elevation.

decay minus a background estimated from the last 0.3 s. All dose response curves (DRCs) were fitted using a general-order kinetics (GOK) function (Guralnik et al., 2015), which has been shown to be flexible and robust for fitting DRCs with different forms (Peng and Li, 2017). We applied the standard rejection criteria (e.g. Jacobs et al., 2006, 2008) as the basic grain selection criteria (Table S3). Besides these, three additional rejection criteria, including the fast ratio (FR) (Durcan and Duller, 2011; Duller, 2012), the dose saturation level (e.g. Thomsen et al., 2016) and the OSL sensitivity, were also tested on our samples, given that a broad dependence of natural D_e and overdispersion (OD) on these factors was observed for all of our samples (Section 4).

Environmental dose rates for all samples were derived from their U, Th and K contents measured using ICP-MS and ICP-OES techniques. Detailed dose rate information for all samples are summarised in Tables S1 and S2.

4. Results and discussion

4.1. Luminescence characteristics

For each of the samples, the quartz grains exhibit significant grain-to-grain variability in terms of OSL decay rate, inherent brightness and the shape of DRC. For grains passing the standard rejection criteria, ~20–30% of grains show OSL signals decaying to < 10% of the initial intensity after 0.2 s stimulation, suggesting the dominance of a fast component; nevertheless, there are also similar proportion of grains exhibit a remnant OSL > 30% of their initial intensities after 0.2 s stimulation, indicating a relatively high proportion of slower components in their OSL (e.g. Fig. S1a). In order to characterise the OSL decay rates for all samples, we calculated the FR of each grain for each sample, using the OSL signals of the natural test doses (T_n) and with the same integrals as proposed by Jacobs et al. (2013) (0–0.02 s for fast component, 0.18–0.22 s for medium and slow components). The median FR for the grains which pass the standard rejection criteria ranges from 4 to 7 for the seven samples. All samples show a broad distribution in FR (mostly range from ~1 to 40), suggesting that the proportion of the fast component varies considerably between grains for all of these samples (e.g. Fig. S1c).

The DRCs of the grains exhibit different shapes and considerable variation in dose saturation levels (e.g. Fig. S1b). When a single saturating exponential function was used to fit the DRCs of all grains, the obtained D_0 value ranged from ~30 to 300 Gy for grains from different

samples, with a median D_0 value of ~120–130 Gy for each sample (e.g. Fig. S1d). Nevertheless, for each sample there are many of the grains whose DRCs are not well represented by a single exponential growth function, for which the D_0 values obtained using single saturating exponential fitting would be inaccurate. To better compare the dose saturation properties of grains with variable forms of DRCs, we used the ratio between the sensitivity-corrected luminescence signals of two different regenerative doses to characterise the dose saturation characteristics of individual grains (also see Li et al., 2016). We name this ratio as the signal growth ratio (SGR), and in this study define it as the ratio between the fitted L_x/T_x values for two arbitrarily chosen regeneration doses of 200 Gy and 50 Gy, derived from the DRC of each grain fitted using the GOK model (i.e. the higher the SGR is, the later the grain is getting saturated). Similar to the apparent D_0, the SGR varies significantly between grains for all samples, corresponding to their very different dose saturation levels (e.g. Fig. S1e).

Cumulative OSL brightness curves (Fig. S2) reveal significant variation in inherent brightness between grains with about 10% of the measured grains yielding ~ 90% of the total OSL signal. The intensity of T_n of the accepted grains (after standard rejection criteria) varies by 4-6 orders of magnitude (e.g. Fig. S1a). The sensitivity of sedimentary quartz grains has been suggested to be associated with multiple factors such as the source origin of the mineral grains and their sedimentary/thermal history (e.g. Li and Wintle, 1992; Pietsch et al., 2008; Sawakuchi et al., 2012; Fitzsimmons, 2011). These factors may also affect other luminescence properties of quartz grains including the relative proportion of the fast component and dose saturation properties, as suggested in previous studies (e.g. Chen et al., 2001; Lai et al., 2008; Gong et al., 2014, 2015). To explore the potential correlation between these luminescence properties, the FRs of quartz grains were compared against their T_n signals and SGRs for our samples (e.g. Fig. S3). We observed moderate positive correlation between FR and T_n (e.g. $\rho = 0.5$ in Fig. S3a) and moderate negative correlation between FR and SGR (e.g. $\rho = -0.4$ in Fig. S3b). This suggests that in general the grains with higher contribution from the fast component would be brighter and saturate earlier, and vice versa.

The positive correlation between FR and T_n is consistent with previous investigations which suggest that the sensitization of the quartz OSL signal (either by repeated dosing/bleaching, heating or inherited from source rock) is mainly related to the fast component (e.g. Preusser et al., 2009; Jeong and Choi, 2012); thus, grains with higher content of the fast component are expected to have a greater sensitivity. Gong et al. (2014, 2015) also observed that for their samples from Chinese deserts the quartz grains with higher content of non-fast components saturate later. This was attributed to the fact that the DRCs of medium and slow components saturate later than that of the fast component (Bailey, 2000b; Singarayer and Bailey, 2003; Rhodes et al., 2006). To check whether this is true for our samples, we examined the variation of SGR as a function of OSL measurement time for the quartz grains (the SGR(t) plot, similar to the D_e (t) plot of Bailey (2000a). Fig. S4 shows examples of two grains with high (> 20) and low (< 2) FR. For both grains, the SGR shows an obvious increasing tendency towards the later integrals, suggesting that the non-fast components saturate later compared to the fast component. This observation also holds true for other grains from our samples. We therefore interpret that the negative correlation between SGR and FR is due to a greater contribution of the non-fast components to the bulk OSL signals of the slowly-decaying grains.

4.2. Dose recovery test

Single-grain dose recovery tests were carried out on samples UH-URB, KPW-2 and KPW-5 to validate the SAR protocol (Fig. S5 and S6). The given doses in the dose recovery tests were close to the natural doses of these samples. The dose recovery ratios (calculated using the central age model (CAM, Galbraith et al., 1999)) for the three samples are 0.97 ± 0.02, 0.99 ± 0.01 and 0.92 ± 0.02 respectively, after application of the standard rejection criteria. These results demonstrate that with our measurement conditions and the standard rejection criteria, we are able to recover a known laboratory dose accurately when the given doses are close to the natural D_es of our samples, except for the oldest sample KPW-5 (which were given a large surrogate natural dose of 234 Gy in the dose recovery test) whose dose recovery ratio was slightly less than unity. Changing preheat and cutheat conditions did not improve the results for KPW-5.

Sample KPW-5 has a high palaeodose and contains a lot of statured or near-saturated grains. It has been suggested that (e.g. Li et al., 2016; Thomsen et al., 2016) for this kind of sample, the measured D_e distribution can be truncated since some early-saturating grains may only be able to record D_es with lower values, and this can lead to underestimation in the dose recovery ratio and D_e estimate. Several studies suggested that removing early-saturating grains can improve the dose recovery ratios and D_e estimates for these samples (Gliganic et al., 2012; Demuro et al., 2015; Thomsen et al., 2016; Guo et al., 2017; Guérin et al., 2017). To test this, we applied a SGR rejection criterion in addition to the standard rejection criteria to the dose recovery dataset of KPW-5, i.e. accept grains only when their SGR values are larger than a threshold. Fig. S5f shows the dose recovery ratio of KPW-5 as a function of the SGR threshold. The dose recovery ratio increases gradually with the chosen SGR above which grains are rejected, while a plateau consistent with unity (at 1σ) has been reached when the SGR threshold is 2.1 or larger. These results suggest that rejecting early-saturating grains can help better recover the given dose for this specific sample. For other younger samples, application of the SGR selection makes no change in the dose recovery ratio (e.g. Fig. S5e). Fig. S6 shows the distribution of measured-to-given dose ratios for grains from UH-URB, KPW-2 (both applied standard rejection criteria) and KPW-5 (applied standard plus SGR rejection criteria). The OD values for the dose recovery results of the three samples are 8%, 7% and 15%, respectively.

Since in the natural D_e analysis we also tested another two rejection criteria—FR and T_n (see below), these two criteria were also tested on the dose recovery results. Figs. S5a–d show the dose recovery ratio as a function of the FR and T_n thresholds for samples UH-URB and KPW-5. For both samples, we observed no dependence of the dose recovery ratio on FR or the intensity of T_n. The results for the latter sample differ from Duller (2012), who observed that application of the FR rejection criterion can improve the dose recovery ratio at higher doses.

4.3. Natural D_e distribution and palaeodose estimation

Application of the standard rejection criteria to all samples results in 86–97% grains being rejected for D_e estimation (Table S3). The criteria that eliminate most grains are associated with the weak inherent brightness (T_n is within 3σ of the BG or relative standard error of T_n > 20%, rejected 71–93% grains), while other criteria generally reject less than 15% grains in total. After application of the standard rejection criteria, five out of the seven samples (UH-URB, UH-LRB, KPW-2, -4 and -5) show medium OD values ranging from 28% to 46%, while other two samples (KPW-1 and -3) yield high OD values of 144% and 92%, respectively.

The OD of the natural D_e dataset is associated with both intrinsic (e.g. luminescence properties (Galbraith et al., 2005)) and extrinsic factors (e.g. microdosimety, partial bleaching, post-depositional mixing). Duller (2012) initially suggested that applying a FR rejection criterion to single-grain datasets can reduce the intrinsic OD by rejecting grains with aberrant behaviours, whereas the efficacy of the FR rejection criterion on natural D_e and its OD has since been shown to be sample dependent (Jacobs et al., 2013; Fu et al., 2015; Feathers, 2015; Trauerstein et al., 2017). To test the rejection based on FR criteria for our samples, we applied different FR rejection threshold to our single-grain datasets. For the five samples with medium OD, the CAM D_e increases with FR threshold until plateauing at a FR threshold of 4–5;

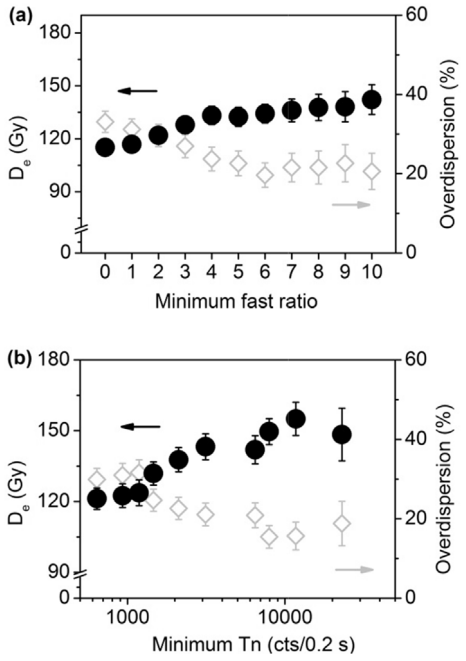

Fig. 3. (a) CAM D_e (filled circles) and OD (open diamonds) of sample UH-URB against the fast ratio rejection threshold. (b) CAM D_e (filled circles) and OD (open diamonds) of sample UH-URB against the T_n rejection threshold.

meanwhile, the OD value also decreases to a plateau at about the same FR threshold (see an example in Fig. 3a). This is similar to the natural D_e data of Fu et al. (2015) and Feathers (2015), which showed that the quartz grains with low FR are likely to yield underestimated D_es, resulting in final D_e underestimation and OD increase. In contrast to Duller (2012) and Feathers (2015), we observed no dependence of the dose recovery ratio on FR (Figs. S5a and b). We therefore deduce that the dependence of natural D_e on FR is unrelated to the performance of the grains in the SAR protocol, rather it is likely to be related to the thermal stability of the non-fast components, which have been shown to be unstable for dating (e.g. Li and Li, 2006; Steffen et al., 2009). To confirm this, we examined the D_e (t) plots and pulse annealing curves of quartz grains with low and high FR. The results show that the non-fast components in our samples yield underestimated D_e compared to the fast component, and grains with lower FR are thermally more unstable than those with higher FR (see details in Figs. S7 and S8). For the two samples with high OD, the dependence of D_e and OD on FR is weak. We infer that this is because the D_e dispersion of these two samples mainly arises from extrinsic factors (bioturbation, see below). Nevertheless, including grains with potential thermal stability problems may obscure the real D_e distribution pattern for these samples.

Since a positive correlation between FR and intrinsic sensitivity has been observed (Fig. S3a), a T_n rejection criterion is also expected to discard unwanted grains which yield underestimated D_es. Fig. 3b shows the D_e and OD of UH-URB as a function of the T_n threshold. As expected, plateaus in D_e and OD are achieved for brighter grains; the plateaus are consistent with those for the FR rejection threshold test (Fig. 3a). But in general, application of the T_n rejection criterion has rejected more grains compared with FR rejection criterion without achieving any refined precision, and there lacks a uniform inter-sample standard for applying the sensitivity rejection criterion. Thus, we prefer the FR rejection criterion to the T_n rejection criterion in this paper.

On the basis of the above arguments, we used the FR as an additional rejection criterion for all of our samples, using a FR threshold value of 5 based on the D_e plateaus for our samples. This FR criterion has rejected ~1%–9% of the grains for different samples in addition to the standard rejection criteria. Given that a dependence of the dose

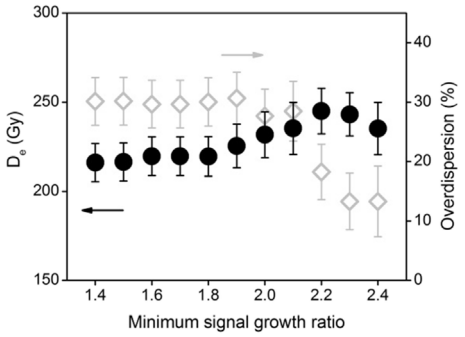

Fig. 4. CAM D_es (filled circles) and OD (open diamonds) of sample KPW-5 against the signal growth ratio rejection threshold, for grains passing the standard rejection criteria and with fast ratio > 5.

recovery ratio on the dose saturation property of grains is observed for sample KPW-5 (Fig. S5f), we've also tested using the SGR as a rejection criterion for our samples, using grains which pass the standard rejection criteria and with FR > 5. We found the use of the SGR rejection criterion does not change the results for the six younger samples, suggesting that the single-grain ages of these samples are negligibly affected by dose saturation; but for the oldest sample KPW 5, the use of a SGR threshold criterion appears to be helpful in removing the bias in the single-grain D_e selection, as indicated by an increase in D_e with increasing SGR threshold and the achievement of a D_e plateau when the SGR threshold is tighten to a value of ~2.0 or higher (Fig. 4). This plateau range is also consistent with that of the dose recovery test for this sample (Fig. S5f). Based on this, we applied a SGR rejection criterion (using a threshold value of 2.1 according to the dose recovery test) in addition to the standard plus FR rejection criteria for sample KPW-5. Application of the SGR threshold criterion has further rejected ~2% of the grains for KPW-5.

The SGR threshold criterion has also been tested on all of the grains passing the standard rejection criteria (i.e. without conducting the FR selection). By doing this, we've identified some grains in our samples which exhibit high dose saturation levels (high SGR) and low D_e values (Fig. S9a). A detailed examination of luminescence properties of these grains reveal that these grains are likely to contain more non-fast components, therefore can yield underestimated D_es due to low thermal stability; application of a FR rejection criterion can reject these grains for D_e estimation (see details in Figs. S9b–d).

Fig. 5 shows the final D_e distributions of all samples as radial plots. After application of the additional rejection criteria (FR or FR & SGR), the OD values for the five mediumly dispersed samples (UH-URB, UH-LRB, KPW-2, -4 and -5) are all reduced (from 28-46% to 23–34%). The OD of these five samples are within the reported values for well-bleached samples (Arnold and Roberts, 2009); and the symmetrical single-grain D_e distributions of them indicate that they are sufficiently bleached. We have therefore applied a CAM to estimate the palaeodoses for these five samples. Samples KPW-1 and KPW-3 present high OD values even after application of the FR rejection criterion (161% and 89%, respectively). These two samples show strong mixing features in their D_e distributions, as evidenced by discrete D_e components being identified in the radial plots (Fig. 5). We deduce that these two samples have experienced bioturbation after deposition, as we've observed plants growing on the outcrop and KPW-1 is also close to the terrace surface (Fig. 2e). A finite mixture model (FMM) (Roberts et al., 2000) was therefore applied to these two samples for palaeodose evaluation (Table S4). A D_e population that comprised the majority (58%) of grains in the D_e distribution is identified for KPW-1, which possibly gives a good estimation for its burial dose. But for KPW-3, two major D_e populations with similar proportion are exhibited in the D_e dataset (42% and 38%, respectively), indicating the sample was severely mixed after deposition and ambiguity exists for identification of a D_e population

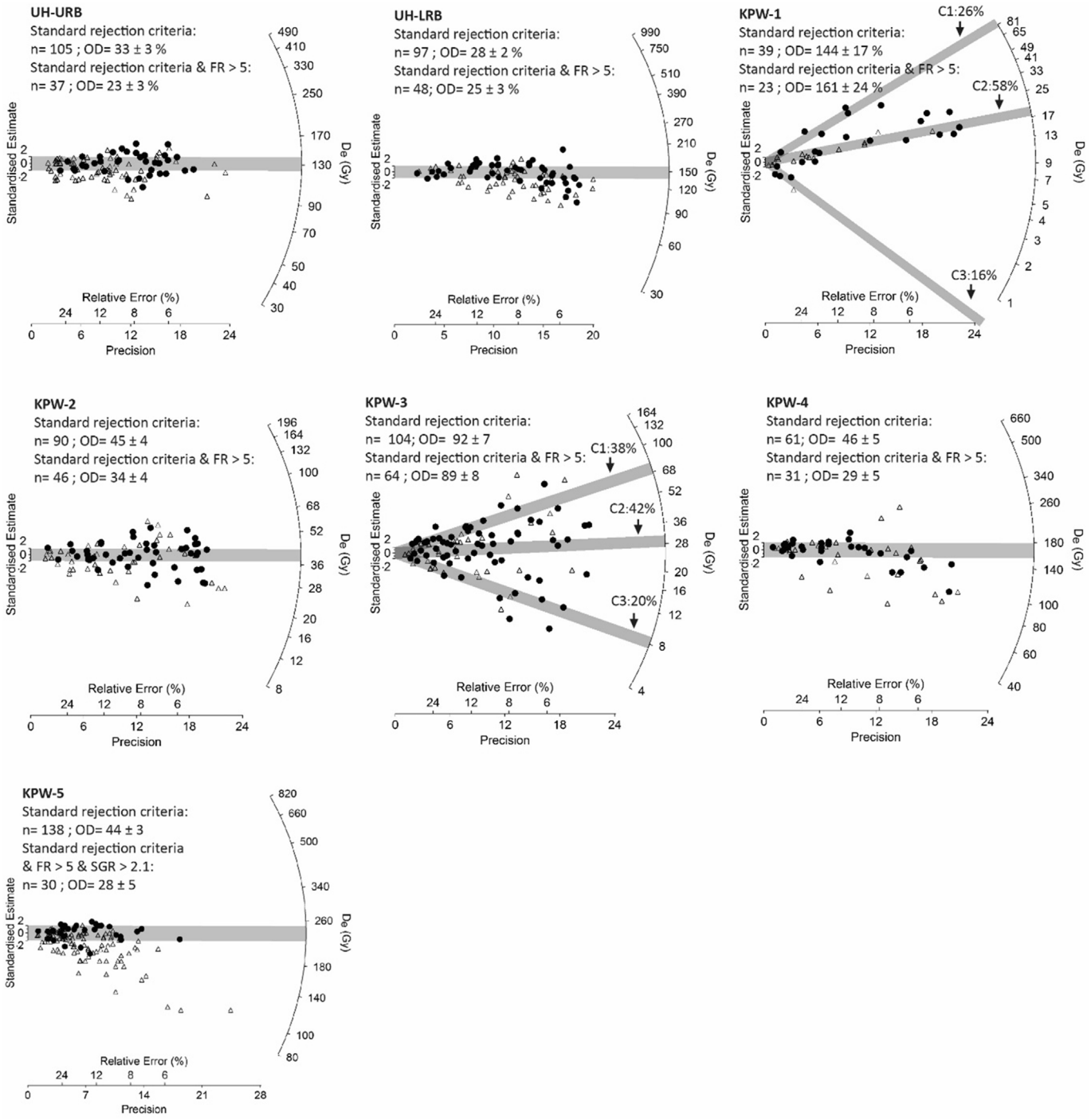
UH-URB
Standard rejection criteria:
n= 105 ; OD= 33 ± 3 %
Standard rejection criteria & FR > 5:
n= 37 ; OD= 23 ± 3 %
UH-LRB
Standard rejection criteria:
n= 97 ; OD= 28 ± 2 %
Standard rejection criteria & FR > 5:
n= 48; OD= 25 ± 3 %
KPW-1
Standard rejection criteria:
n= 39 ; OD= 144 ± 17 %
Standard rejection criteria & FR > 5:
n= 23 ; OD= 161 ± 24 %
C1:26%
C2:58%
C3:16%
KPW-2
Standard rejection criteria:
n= 90 ; OD= 45 ± 4
Standard rejection criteria & FR > 5:
n= 46 ; OD= 34 ± 4
KPW-3
Standard rejection criteria:
n= 104; OD= 92 ± 7
Standard rejection criteria & FR > 5:
n= 64 ; OD= 89 ± 8
C1:38%
C2:42%
C3:20%
KPW-4
Standard rejection criteria:
n= 61; OD= 46 ± 5
Standard rejection criteria & FR > 5:
n= 31 ; OD= 29 ± 5
KPW-5
Standard rejection criteria:
n= 138 ; OD= 44 ± 3
Standard rejection criteria
& FR > 5 & SGR > 2.1:
n= 30 ; OD= 28 ± 5
Standardised Estimate
De (Gy)
Relative Error (%)
Precision

Fig. 5. Radial plots showing the single-grain D_e distributions of all samples. All datapoints are for grains passing the standard rejection criteria. The closed circles and open triangles represent grains accepted and rejected by additional rejection criteria (FR > 5 & SGR > 2.1 for KPW-5 and FR > 5 for other samples), respectively. The shaded bands for samples UH-URB, UH-LRB, KPW-2, -4 and -5 are centred on their weighted mean D_es calculated using the CAM (for grains passing the standard plus additional rejection criteria). The shaded bands for samples KPW-1 and -3 are centred on the weighted mean D_es for each grain population obtained using the FMM (for grains passing the standard plus additional rejection criteria).

related to deposition. We infer that the two grain populations may originate from two stratigraphic units representing two river aggradation events (i.e. grains from one unit were mixed into the other due to bioturbation), and we tentatively used the D_e values of the two major populations to give two potential depositional ages for this sample. These ages were treated with caution when doing the climate interpretation. Table S1 gives a summary of the palaeodoses and ages of all samples.

4.4. Chronologies of the terraces and their implications

The final ages for all of the samples are compared with glacial-interglacial cycles (Fig. 6). The two samples collected from adjacent terraces of the upper Hunter River indicate two aggradational episodes of the river. Sample UH-LRB collected from the silty clay immediately above the coarse-gravel unit of the Razorback lower terrace yields an age of 93.9 ± 5.7 ka, suggesting a floodplain accretion event occurred at mid-to-late MIS 5. Another sample UH-UHB collected from the silty

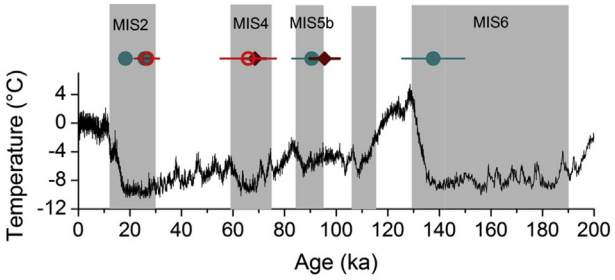

Fig. 6. Plot showing a comparison of the OSL ages with MIS stages and late Quaternary temperature anomaly recovered from Antarctic ice core (Jouzel et al., 2007). Grey bars represent glacial and stadial episodes. Diamonds represent ages of samples from the Razorback terraces. Circles represent ages of samples from Kingdon Ponds terrace. The open circles indicate two potential ages of the severely mixed sample KPW-3.

clay deposits of the Razorback upper terrace yields an age of 65.0 ± 4.1 ka, suggesting a later valley floor aggradation occurred in MIS 4. Further dating of the upper section of the two terraces will build more detailed age structures for these terraces.

The ages of the five samples collected from the Kingdon Ponds terrace are consistent with their stratigraphic order. The lowest sample from Unit B comprising of silty clay yields an age of 137.7 ± 12.1 ka, suggesting an episode of floodplain accretion close to modern river level occurred in late MIS 6. The bottom of the coarse gravel unit (Unit C1; Fig. 2e) lying above Unit B is dated to be 90.5 ± 7.6 ka, suggesting a coarse-gravel bed river occupied this valley elevation at mid-to-late MIS 5, similar to the timing of the Razorback lower terrace in adjacent valley. A higher sample from Unit D1 returns two potential ages of 65.8 ± 10.8 ka and 26.6 ± 4.8 ka. The older age may represent a depositional event chronologically similar to the formation of the Razorback upper terrace. The younger age is indistinguishable with the age of the overlying debris deposits (Unit E1, dated to 25.7 ± 1.9 ka), atop which a silty clay unit (Unit F1) is aged at 18.3 ± 2.0 ka. These stratigraphic units with similar ages may reflect different phases of valley floor aggradation (including channel and floodplain deposition and alluvial fan deposition) occurred intermittently during MIS 2, albeit the age of Unit D1 (obtained from the severely mixed sample KPW-3) may need to be treated with caution.

Nott et al. (2002) and Nanson et al. (2003) have investigated large coastal draining rivers in NSW and extended the fluvial records of southeastern Australian coastal catchments to ~ 100 ka. Based on TL dating of fluvial sediments, these studies argued for an enhanced pluvial episode at (mid-to-late) MIS 5 and a declined fluvial activity at LGM. Broadly similar conclusions were achieved in earlier investigations on fluvial sediments in the Riverine Plain based on TL or OSL dating (e.g. Page et al., 1996; Kemp and Rhodes, 2010). Recently, a study on the Willandra Lakes on the Riverine Plain suggested these lakes were fed by the palaeo-sub branch of the Lachlan River (arising in the GDR) and maintained a high lake stand at the LGM (Kemp et al., 2017). Similar results by Mueller et al. (submitted) have shown elevated discharge (relative to today) on the Murrumbidgee River at the LGM. In comparison, the fluvial terraces in the upper Hunter catchment also record fluvial aggradation in mid-to-late MIS 5 and the enhanced alluvial sedimentation in MIS 2, as recorded in the Kingdon Ponds terrace, which may be closely related to the LGM high lake level and river activity phase of the Riverine Plain.

The chronologies obtained in this study appear to suggest that all the river aggradation phases in the upper Hunter catchment occurred in glacial or stadial periods (MIS 6, MIS 5b, MIS 4 and MIS 2) (Fig. 6). In Australia, fluvial sedimentation tends to be dominated by sediment availability (e.g. Nanson et al., 1992; Page et al., 1996). A potential major source of sediment is the nearby ranges which have elevations of ~1000–1500 m a.s.l. A recent study of Slee and Shulmeister (2015) has identified extensive periglacial landforms in eastern Australian mountain regions including the upper Hunter catchment. These periglacial landforms, whist undated, provide evidence for strong freeze-thaw processes throughout the late Quaternary and presumably have formed in the cold periods with adequate moisture. An increased sediment supply provided by the strong periglacial activities, together with increased runoff due to seasonal snowmelt (Reinfelds et al., 2014) and decreased sediment residence time due to variation of vegetation (Dosseto et al., 2010) during the cold episodes, is very likely to drive the aggradation of valley floors. If this hypothesis is true, there must be a regional similarity between the long-term fluvial records in areas affected by past periglacial processes. More chronological studies of other fluvial archives in large coastal draining catchments in southeastern Australia, such as the Shoalhaven River, should further test this hypothesis.

5. Conclusions

Chronologies of three fluvial terraces in the upper Hunter catchment in southeastern Australia were investigated using single-grain quartz OSL dating. Detailed luminescence investigations revealed some correlation between multiple luminescence properties of individual grains and their D_e values. Application of additional single-grain rejection criteria were found to reduce overdispersion arising from intrinsic factors and improve the dating results. Our dating results extended the fluvial record in southeastern Australia to MIS 6 and set a hypothesis that fluvial aggradation in the upper Hunter catchment is associated with glacial or stadial periods, which may be explained by enhanced sediment supply to the catchment resulting from strong periglacial activities during the cold episodes.

Acknowledgements

This study was supported by an Australian Research Council Discovery Project grant (DP110103081) to TC. XF thanks the ARC Laureate Fellowship grant (FL130100116) to Professor Richard Roberts for financial support for the LED 2017 conference. We also thank John Janson and Luke Gliganic for their support in the collection of the Upper Hunter at Razorback samples, Luke Gliganic for preparation of these samples and to Daniela Mueller for preparing some of the KPW samples. We also would like to thank Bo Li and Zenobia Jacobs for giving helpful comments on the early results of this study. This paper also benefitted by the comments of an anonymous reviewer.

Appendix A. Supplementary data

Supplementary data related to this article can be found at http://dx.doi.org/10.1016/j.quageo.2018.06.002.

References

Arnold, L.J., Roberts, R.G., 2009. Stochastic modelling of multi-grain equivalent dose (De) distributions: implications for OSL dating of sediment mixtures. Quat. Geochronol. 4, 204–230.
Bailey, R.M., 2000a. The interpretation of quartz optically stimulated luminescence equivalent dose versus time plots. Radiat. Meas. 32, 129–140.
Bailey, R.M., 2000b. The slow component of quartz optically stimulated luminescence. Radiat. Meas. 32, 233–246.
Brooks, A.P., Brierley, G.J., Millar, R.G., 2003. The long-term control of vegetation and woody debris on channel and flood-plain evolution: insights from a paired catchment study in southeastern Australia. Geomorphology 51, 7–29.
Chen, G., Murray, A.S., Li, S.-H., 2001. Effect of heating on the quartz dose-response curve. Radiat. Meas. 33, 59–63.
Cohen, T.J., Nanson, G.C., 2008. Topographically associated but chronologically disjunct late Quaternary floodplains and terraces in a partly confined valley, south-eastern Australia. Earth Surf. Process. Landforms 33, 424–443.
Demuro, M., Arnold, L.J., Parés, J.M., Sala, R., 2015. Extended-range luminescence chronologies suggest potentially complex bone accumulation histories at the Early-to-Middle Pleistocene palaeontological site of Huéscar-1 (Guadix-Baza basin, Spain). Quat. Int. 389, 191–212.

Dosseto, A., Hesse, P.P., Maher, K., Fryirs, K., Turner, S., 2010. Climatic and vegetation control on sediment dynamics during the last glacial cycle. Geology 38, 395–398.
Duller, G.A.T., 2012. Improving the accuracy and precision of equivalent doses determined using the optically stimulated luminescence signal from single grains of quartz. Radiat. Meas. 47, 770–777.
Duller, G.A.T., 2003. Distinguishing quartz and feldspar in single grain luminescence measurements. Radiat. Meas. 37, 161–165.
Durcan, J.A., Duller, G.A.T., 2011. The fast ratio: a rapid measure for testing the dominance of the fast component in the initial OSL signal from quartz. Radiat. Meas. 46, 1065–1072.
Feathers, J., 2015. Luminescence dating at Diepkloof Rock Shelter – new dates from single-grain quartz. J. Archaeol. Sci. 63, 164–174.
Fitzsimmons, K., 2011. An assessment of the luminescence sensitivity of Australian quartz with respect to sediment history. Geochronometria 38, 199–208.
Fryirs, K., Brierley, G., 1998. The character and age structure of valley fills in upper Wolumla Creek catchment, south coast, New South Wales, Australia. Earth Surf. Process. Landforms 23, 271–287.
Fryirs, K., Brierley, G.J., 2010. Antecedent controls on river character and behaviour in partly confined valley settings: upper Hunter catchment, NSW, Australia. Geomorphology 117, 106–120.
Fu, X., Cohen, T.J., Arnold, L.J., 2017a. Extending the record of lacustrine phases beyond the last interglacial for Lake Eyre in central Australia using luminescence dating. Quat. Sci. Rev. 162, 88–110.
Fu, X., Li, S.-H., Li, B., Fu, B., 2017b. A fluvial terrace record of late Quaternary folding rate of the Anjihai anticline in the northern piedmont of Tian Shan, China. Geomorphology 278, 91–104.
Fu, X., Li, S.-H., Li, B., 2015. Optical dating of aeolian and fluvial sediments in north Tian Shan range, China: luminescence characteristics and methodological aspects. Quat. Geochronol. 30, 161–167.
Galbraith, R.F., Roberts, R.G., Laslett, G.M., Yoshida, H., Olley, J.M., 1999. Optical dating of single and multiple grains of quartz from Jinmium rock shelter, northern Australia: Part I, experimental design and statistical models. Archaeometry 41, 339–364.
Galbraith, R.F., Roberts, R.G., Yoshida, H., 2005. Error variation in OSL palaeodose estimates from single aliquots of quartz: a factorial experiment. Radiat. Meas. 39, 289–307.
Gliganic, L.A., Jacobs, Z., Roberts, R.G., 2012. Luminescence characteristics and dose distributions for quartz and feldspar grains from Mumba rockshelter, Tanzania. Archaeological and Anthropological Sciences 4, 115–135.
Gong, Z., Sun, J., Lü, T., 2015. Investigating the components of the optically stimulated luminescence signals of quartz grains from sand dunes in China. Quat. Geochronol. 29, 48–57.
Gong, Z., Sun, J., Lü, T., Tian, Z., 2014. Investigating the optically stimulated luminescence dose saturation behavior for quartz grains from dune sands in China. Quat. Geochronol. 22, 137–143.
Guérin, G., Frouin, M., Tuquoi, J., Thomsen, K.J., Goldberg, P., Aldeias, V., Lahaye, C., Mercier, N., Guibert, P., Jain, M., Sandgathe, D., McPherron, S.J.P., Turq, A., Dibble, H.L., 2017. The complementarity of luminescence dating methods illustrated on the Mousterian sequence of the Roc de Marsal: a series of reindeer-dominated, Quina Mousterian layers dated to MIS 3. Quat. Int. 433, 102–115.
Guo, Y.-J., Li, B., Zhang, J.-F., Yuan, B.-Y., Xie, F., Roberts, R.G., 2017. New ages for the upper palaeolithic site of Xibaimaying in the Nihewan basin, northern China: implications for small-tool and microblade industries in north-east Asia during marine Isotope stages 2 and 3. J. Quat. Sci. 32, 540–552.
Guralnik, B., Li, B., Jain, M., Chen, R., Paris, R.B., Murray, A.S., Li, S.-H., Pagonis, V., Valla, P.G., Herman, F., 2015. Radiation-induced growth and isothermal decay of infrared-stimulated luminescence from feldspar. Radiat. Meas. 81, 224–231.
Jacobs, Z., Duller, G.A.T., Wintle, A.G., 2006. Interpretation of single grain De distributions and calculation of De. Radiat. Meas. 41, 264–277.
Jacobs, Z., Hayes, E.H., Roberts, R.G., Galbraith, R.F., Henshilwood, C.S., 2013. An improved OSL chronology for the Still Bay layers at Blombos Cave, South Africa: further tests of single-grain dating procedures and a re-evaluation of the timing of the Still Bay industry across southern Africa. J. Archaeol. Sci. 40, 579–594.
Jacobs, Z., Roberts, R.G., Galbraith, R.F., Deacon, H.J., Grün, R., Mackay, A., Mitchell, P., Vogelsang, R., Wadley, L., 2008. Ages for the Middle stone age of southern Africa: implications for human behavior and dispersal. Science 322, 733–735.
Jeong, G.Y., Choi, J., 2012. Variations in quartz OSL components with lithology, weathering and transportation. Radiat. Meas. 10, 320–326.
Jouzel, J., Masson-Delmotte, V., Cattani, O., Dreyfus, G., Falourd, S., Hoffmann, G., Minster, B., Nouet, J., Barnola, J.M., Chappellaz, J., Fischer, H., Gallet, J.C., Johnsen, S., Leuenberger, M., Loulergue, L., Luethi, D., Oerter, H., Parrenin, F., Raisbeck, G., Raynaud, D., Schilt, A., Schwander, J., Selmo, E., Souchez, R., Spahni, R., Stauffer, B., Steffensen, J.P., Stenni, B., Stocker, T.F., Tison, J.L., Werner, M., Wolff, E.W., 2007. Orbital and Millennial Antarctic climate variability over the past 800,000 years. Science 317, 793–796.
Kemp, J., Pietsch, T., Gontz, A., Olley, J., 2017. Lacustrine-fluvial interactions in Australia's riverine plains. Quat. Sci. Rev. 166, 352–362.
Kemp, J., Rhodes, E.J., 2010. Episodic fluvial activity of inland rivers in southeastern Australia: palaeochannel systems and terraces of the Lachlan River. Quat. Sci. Rev. 29, 732–752.
Kreutzer, S., Dietze, M., Burow, C., Fuchs, M.C., Schmidt, C., Fischer, M., Friedrich, J., 2017. Luminescence: Comprehensive Luminescence Dating Data Analysis. R package version 0.7.5. https://CRAN.R-project.org/package=Luminescence.
Lai, Z., Brückner, H., Fülling, A., Zöller, L., 2008. Effects of thermal treatment on the growth curve shape for OSL of quartz extracted from Chinese loess. Radiat. Meas. 43, 763–766.
Li, B., Jacobs, Z., Roberts, R.G., 2016. Investigation of the applicability of standardised growth curves for OSL dating of quartz from Haua Fteah cave, Libya. Quat. Geochronol. 35, 1–15.
Li, B., Li, S.-H., 2006. Comparison of De estimates using the fast component and the medium component of quartz OSL. Radiat. Meas. 41, 125–136.
Li, S.-H., Wintle, A.G., 1992. Luminescence sensitivity change due to bleaching of sediments. Nucl. Tracks Radiat. Meas. 20, 567–573.
Meng, Y.M., Zhang, J.F., Qiu, W.L., Fu, X., Guo, Y.J., Zhou, L.P., 2015. Optical dating of the Yellow River terraces in the Mengjin area (China): first results. Quat. Geochronol. 30, 219–225.
Mueller, D., Jacobs, Z., Cohen, T.J., Price, D.M., Reinfelds, I.V., Shulmeister, J. Revisiting an arid LGM using fluvial archives: A luminescence chronology for palaeochannels of the Murrumbidgee River, southeastern Australia. J. Quat. Sci., submitted.
Murray, A.S., Wintle, A.G., 2000. Luminescence dating of quartz using an improved single-aliquot regenerative-dose protocol. Radiat. Meas. 32, 57–73.
Nanson, G.C., Cohen, T.J., Doyle, C.J., Price, D.M., 2003. Alluvial evidence of major late-Quaternary climate and flow-regime changes on the coastal rivers of New South Wales, Australia. In: Gregory, K., Benito, G. (Eds.), Palaeohydrology: Understanding Global Change. Wiley, Chichester, pp. 233–258.
Nanson, G.C., Price, D.M., Short, S.A., 1992. Wetting and drying of Australia over the past 300 ka. Geology 20, 791–794.
Nott, J., Price, D., Nanson, G., 2002. Stream response to Quaternary climate change: evidence from the Shoalhaven River catchment, southeastern highlands, temperate Australia. Quat. Sci. Rev. 21, 965–974.
Page, K., Nanson, G., Price, D., 1996. Chronology of Murrumbidgee River palaeochannels on the Riverine Plain, southeastern Australia. J. Quat. Sci. 11, 311–326.
Page, K.J., Kemp, J., Nanson, G.C., 2009. Late quaternary evolution of Riverine Plain paleochannels, southeastern Australia. Aust. J. Earth Sci. 56, S19–S33.
Peng, J., Li, B., 2017. Single-aliquot regenerative-dose (SAR) and standardised growth curve (SGC) equivalent dose determination in a batch model using the R Package 'numOSL'. Ancient TL 35, 32–53.
Pietsch, T.J., Olley, J.M., Nanson, G.C., 2008. Fluvial transport as a natural luminescence sensitiser of quartz. Quat. Geochronol. 3, 365–376.
Preusser, F., Chithambo, M.L., Götte, T., Martini, M., Ramseyer, K., Sendezera, E.J., Susino, G.J., Wintle, A.G., 2009. Quartz as a natural luminescence dosimeter. Earth Sci. Rev. 97, 184–214.
Reinfelds, I., Swanson, E., Cohen, T., Larsen, J., Nolan, A., 2014. Hydrospatial assessment of streamflow yields and effects of climate change: snowy Mountains, Australia. J. Hydrol. 512, 206–220.
Rhodes, E.J., Singarayer, J.S., Raynal, J.-P., Westaway, K.E., Sbihi-Alaoui, F.Z., 2006. New age estimates for the Palaeolithic assemblages and Pleistocene succession of Casablanca, Morocco. Quat. Sci. Rev. 25, 2569–2585.
Roberts, R.G., Galbraith, R.F., Yoshida, H., Laslett, G.M., Olley, J.M., 2000. Distinguishing dose populations in sediment mixtures: a test of single-grain optical dating procedures using mixtures of laboratory-dosed quartz. Radiat. Meas. 32, 459–465.
Sawakuchi, A.O., Guedes, C.C.F., DeWitt, R., Giannini, P.C.F., Blair, M.W., Nascimento, D.R., Faleiros, F.M., 2012. Quartz OSL sensitivity as a proxy for storm activity on the southern Brazilian coast during the Late Holocene. Quat. Geochronol. 13, 92–102.
Singarayer, J.S., Bailey, R.M., 2003. Further investigations of the quartz optically stimulated luminescence components using linear modulation. Radiat. Meas. 37, 451–458.
Slee, A., Shulmeister, J., 2015. The distribution and climatic implications of periglacial landforms in eastern Australia. J. Quat. Sci. 30, 848–858.
Steffen, D., Preusser, F., Schlunegger, F., 2009. OSL quartz age underestimation due to unstable signal components. Quat. Geochronol. 4, 353–362.
Thomsen, K.J., Murray, A.S., Buylaert, J.P., Jain, M., Hansen, J.H., Aubry, T., 2016. Testing single-grain quartz OSL methods using sediment samples with independent age control from the Bordes-Fitte rockshelter (Roches d'Abilly site, Central France). Quat. Geochronol. 31, 77–96.
Trauerstein, M., Lowick, S.E., Preusser, F., Veit, H., 2017. Testing the suitability of dim sedimentary quartz from northern Switzerland for OSL burial dose estimation. Geochronometria 44, 66–76.
Zhang, J.F., Qiu, W.L., Li, R.Q., Zhou, L.P., 2009. The evolution of a terrace sequence along the Yellow River (HuangHe) in Hequ, Shanxi, China, as inferred from optical dating. Geomorphology 109, 54–65.